Results in Physics 8 (2018) 93–98

Contents lists available at ScienceDirect

Results in Physics

journal homepage: www.journals.elsevier.com/results-in-physics

Study of structural phase transformation and hysteresis behavior of inverse-spinel α-ferrite nanoparticles synthesized by co-precipitation method

Shadab Dabagh [a], Kashif Chaudhary [a,b,*], Zuhaib Haider [a], Jalil Ali [a,b]

[a] Laser Center, Ibnu Sina Institute for Scientific and Industrial Research, Universiti Teknologi Malaysia, 81310 UTM Johor Bahru, Johor, Malaysia
[b] Physics Department, Faculty of Science, Universiti Teknologi Malaysia, 81310 UTM Johor Bahru, Johor, Malaysia

ARTICLE INFO

Article history:
Received 8 November 2017
Received in revised form 27 November 2017
Accepted 28 November 2017
Available online 1 December 2017

Keywords:
Co-precipitation method
XRD
Spinel ferrites
VSM
TEM

ABSTRACT

Substitution of cobalt (Co^{2+}) ions in cobalt ferrite ($CoFe_2O_4$) with copper (Cu^{2+}) and aluminum (Al^{3+}) ions allows variations in their electric and magnetic properties which can be optimized for specific applications. In this article, synthesis of inverse-spinel $Co_{1-x}Cu_xFe_{2-x}Al_xO_4$ ($0.0 \leq x \leq 0.8$) nanoparticles by substituting Cu^{2+} and Al^{3+} ions in $CoFe_2O_4$ via co-precipitation method is reported. By controlling copper and aluminum (Cu-Al) substituent ratio, the magnetic moment and coercivity of synthesized cobalt ferrite nanoparticles is optimized. The role of substituents on the structure, particle size, morphology, and magnetic properties of nano-crystalline ferrite is investigated. The $Co_{1-x}Cu_xFe_{2-x}Al_xO_4$ ($0.0 \leq x \leq 0.8$) nanoparticles with crystallite size in the range of 23.1–26.5 nm are observed, 26.5 nm for $x = 0.0$–23.1 nm for $x = 0.8$. The inverse-spinel structure of synthesized $Co_{1-x}Cu_xFe_{2-x}Al_xO_4$ ($0.0 \leq x \leq 0.8$) nanoparticles is confirmed by characteristic vibrational bands at tetrahedral and octahedral sites using Fourier transform infrared spectroscopy. A decreases in coercive field and magnetic moment is observed as Cu-Al contents are increased ($x = 0.0$–0.8). The positive anisotropy of synthesized particles $Co_{1-x}Cu_xFe_{2-x}Al_xO_4$ ($0.0 \leq x \leq 0.8$) is obtained in the range 1.96×10^5 J/m^3 for $x = 0.0$ to 0.29×10^5 J/m^3 for $x = 0.8$.

Introduction

Cobalt ferrite nanocrystals are promising materials for numerous applications as high-density magnetic recording, ferro fluids technology, biomedical, and magneto-optical devices due to high coercivity and permeability, excellent chemical stability and mechanical hardness [1]. The magnetic properties of these ferrite nano-particles are crucially dependent on the size, shape and purity [2,3]. The spinel – type ferrite with general formula MFe_2O_4 (M = Ni^{2+}, Co^{2+}, Cu^{2+}, etc.) have great potential in different technological application due to their outstanding optical, electrical, and magnetic characteristics. Ferrites with spinel–type structure involves two sublattice tetrahedral site and octahedral site occupied by the trivalent Fe^{3+} ions [4]. Therefore, by substituting these type of divalent cations, it is possible to optimize the basic magnetic characteristics of spinel type ferrites by controlling the size and shape of nanoparticles [4]. Karimi et al. investigated the effect of Dysprosium (Dy) doping in $CoFe_2O_4$ and an increase in the coercive field and a decrease in saturation magnetization (M_s) has reported as a result of Dy doping up to $x = 0.05$ [5]. Monaji et al. studied the structural, morphological and magnetic properties of Zr-doped Co spinel ferrite. An increase in M_s of $Co_{1+x}Zr_xFe_{2-2x}O_4$, was observed with increase in Zr content [6]. Samad et al. studied the effect of Zn-Al substitution on the structural and magnetic properties of Coblat ferrite in an attempt to make it more suitable for high-density recording media applications [7]. In another study, Sontu et al. observed a decrease in M_s and coercivity (H_c) with increasing Ni^{2+} substitution in $Co_{1-x}Ni_xFe_2O_4$ nanoparticles [8]. Several routes such as sol–gel, auto-combustion [9,10], high-energy ball milling, micro-emulsion technique, co-precipitation method, hydrothermal, combustion method, and spray pyrolysis, have been used to fabricate nanoparticles. The co-precipitation synthesis route has advantages over others synthetic techniques, [11,12] due to low cost and easy preparation. In present study ferrites nano-particles are synthesized by substituting Cu^{2+} and Al^{3+} ions into the $CoFe_2O_4$ lattice in different ratios in order to understand the role of the substituents towards the physical properties

* Corresponding author at: Laser Center, Ibnu Sina Institute for Scientific and Industrial Research, Universiti Teknologi Malaysia, 81310 UTM Johor Bahru, Johor, Malaysia.
E-mail address: kashif@utm.my (K. Chaudhary).

https://doi.org/10.1016/j.rinp.2017.11.033
2211-3797/

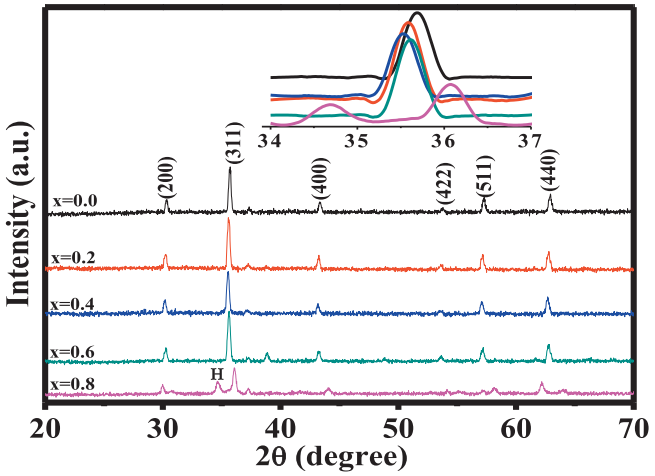

Fig. 1. X-ray diffraction patterns of $Co_{1-x}Cu_xFe_{2-x}$ Al_xO_4 nano-particles.

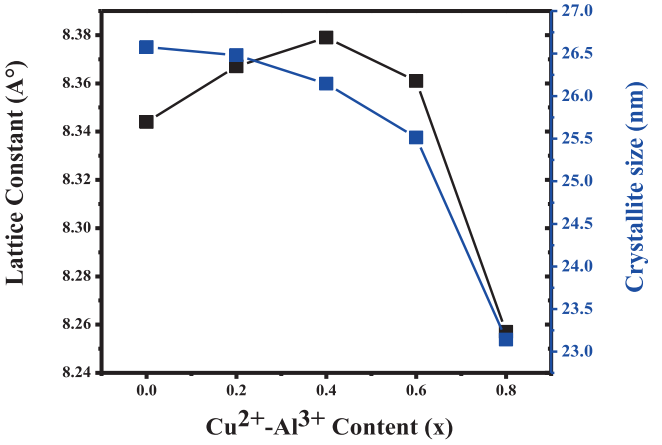

Fig. 2. Variation of lattice constant "a" and crystallite size "D_{xrd}" with respect to increase in Cu^{2+}-Al^{3+} content.

of basic ferrites and the mechanism behind in order to optimize the electric and magnetic response for targeted applications. The role of thermal process and substituents (Cu^{2+} and Al^{3+}) on structural phase transformation and hysteresis behavior on inverse-spinel ferrite nanoparticles is investigated in detail.

Experimental

$Co_{1-x}Cu_xFe_{2-x}Al_xO_4$ ferrites nano-particles with different substitution ratios as (x = 0.0, 0.2, 0.4, 0.6 and 0.8) are tailored using co-precipitation method. Analytical grade cobalt (III) acetate ($Co(CH_3COO)_2{\cdot}4H_2O$(99%)), copper (II) nitrate ($Cu(NO_3)_2{\cdot}6H_2O$ (98.5%)),iron (III) nitrate ($Fe(NO_3)_3{\cdot}9H_2O$(98.5%)) and aluminum nitrate ($Al(NO_3)_3{\cdot}9H_2O$(98.5%)) are used as starting materials to produce Fe^{3+}, Co^{2+}, Al^{3+}, Cu^{2+} ions in solution. The weighted amount of parent materials are dissolved in de-ionized water with calculated stoichiometric ratio. The solution is heated to 80 °C with continuous stirring and the NaOH solution is added drop-wise into reactant solution in order to maintain the pH of the solution between 11.5 and 12.0. Precipitates are washed for several times and dried in oven at 100 °C for 10 h. Phase identification of the prepared nanopowders is performed by X-ray diffraction (XRD). Fourier transform infrared (FTIR) spectra are captured using Perkin Elmer 5DX FTIR and the static magnetic measurements are recorded using Lake Shore 7303–9309 vibrating sample magnetometer (VSM) at room temperature.

Results

Fig. 1 shows X-ray diffraction (XRD) spectrographs of synthesized $Co_{1-x}Cu_xFe_{2-x}Al_xO_4$ $(0.0 \leq x \leq 0.8)$ nano ferrite particles. The spectral peaks located over 2θ range 20–70° associated to the crystalline planes (2 2 0), (3 1 1), (2 2 2), (4 0 0), (4 2 2), (5 1 1), and (4 4 0) are observed in XRD spectra which infers the presence of cubic spinel ferrite structure. A comparison between the X-ray diffraction peaks positions obtained from synthesized cobalt ferrite with standard cobalt ferrite structure is presented in Table 1. It is observed that all the experimental observed peaks are well matched with standard cobalt ferrite which confirms the formation of cobalt ferrite [13].

A spectral peak labeled by 'H' as shown inset in Fig. 1 associated to hematite α-Fe_2O_3 is observed for $Co_{0.2}Cu_{0.8}Fe_{0.2}Al_{0.8}O_4$ nanoparticles with ratio x = 0.8. High concentration of Al ions causes incomplete conversion of Fe_2O_3 into ferrite due to higher melting point of Al which leads to formation of second phase α-Fe_2O_3. By using Scherrer's formula, the average particle sizes of the ferrite particle is determined using (3 1 1) crystallographic plane. The crystallite size varies in the range of 23.1–26.5 nm with Cu-Al substitution for (x = 0.0, 0.2, 0.4, 0.6 and 0.8) as shown in Fig. 2, which ae much smaller in size as compared to reported by other researcher (36.6–69.4 nm and 67 nm) [14,15]. The reduction in the size of magnetic materials gives novel characteristics (Superparamagnetism) as compared to the bulk materials, due to small volume or high surface/volume ratio (spin canting.

Table 2 represents the estimated values of lattice constant (a), cell volume (V) jump length (L) and X-ray density (d_x) of synthesized spinel ferrite nanoparticles.

The shift in diffraction peaks is observed which due to metal ions substitution. The lattice parameter 'a' as listed in Table 2 suggested an increase in lattice constant with increase in Cu-Al contents up to x = 0.4 due to smaller ionic radius of Co^{2+} (0.67 Å) as compared to the ionic radius of Cu^{2+} (0.87 Å). A decrease in 'a' with increase in Cu-Al contents for x = 0.6 and 0.8 is due to the preferential occupation of Al^{3+}(0.51 Å) ions at tetrahedral and octahedral sites by replacing Fe^{3+}(0.67 Å) ions and due to partial oxidation of Cu^{2+} to Cu^{3+} of larger ionic radius and loss of Cu contents, which

Table 1
A comparison of standard and experimental interplanar spacing, d and 2θ values with their respective diffraction (*hkl*) planes.

2θ Standard value [13]	2θ Experimental value	d Standard value [13]	d Experimental value	Diffraction planes *(hkl)*
30.28	30.215	2.94	2.955	220
35.68	35.583	2.51	2.52	311
43.34	43.22	2.08	2.09	400
53.77	53.58	1.70	1.708	422
57.15	57.11	1.60	1.61	511
62.89	62.72	1.47	1.48	440

Table 2
Structural parameters of the synthesized $Co_{1-x}cu_xfe_{2-x}$ al_xo_4 ($0.0 \leq x \leq 0.8$) at 900 °C temperature.

Composition	ν_t (cm^{-1})	ν_o (cm^{-1})	D_{XRD} (nm)	Lattice const. (a) Å	Cell vol. (V) (Å ^{3})	X-ray density (ρx-ray) (g/cm^{-3})	Jump length (L) Å
$CoFe_2O_4$	609.07	368.38	26.57	8.34	580.92	5.36	2.945
$Co_{0.8}Cu_{0.2}Fe_{1.8}Al_{0.2}O_4$	603.06	380.70	26.48	8.36	585.74	6.54	2.953
$Co_{0.6}Cu_{0.4}Fe_{1.6}Al_{0.4}O_4$	598.25	386.11	26.14	8.37	588.26	6.04	2.957
$Co_{0.4}Cu_{0.6}Fe_{1.4}Al_{0.6}O_4$	589.24	387.92	25.51	8.36	584.48	6.33	2.951
$Co_{0.2}Cu_{0.8}Fe_{1.2}Al_{0.8}O_4$	587.48	381.91	23.14	8.25	562.94	6.46	2.914

leads to contraction of lattice [16]. Similar lattice contraction has reported by Tirupanyam *et. al.* in Mn–Ni ferrite due to presence of α-Fe_2O_3 [16]. In Fig. 3, variation in jump length, as a function of copper-aluminum contents (x) in $Co_{1-x}Cu_xFe_{2-x}Al_xO_4$ are presented. A decrease in jump length is observed with increase in Cu-Al doping [17]. The interaction between Fe^{2+} and Fe^{3+} ions at octahedral sites reduces the iron ion concentration with increase in Cu-Al concentration, which may attribute to the replacement of Cu^{2+} and Al^{3+} ions in the tetrahedral and octahedral sites of crystal structure.

The presence of characteristic vibrational bands of the tetrahedral and octahedral sites in FTIR spectra as shown in Fig. 4, confirms the formation inverse-spinel $Co_{1-x}Cu_xFe_{2-x}Al_xO_4$ ($0.0 \leq x \leq 0.8$) structure of ferrites [1]. Four characteristics bands in FTIR ferrites spectra are observed in the range of 200–700 cm^{-1} which are categorized into two groups as two high-frequency bands and one low-frequency bands [4]. The higher frequency absorption band, ν_o around 400 cm^{-1} is associated to octahedral complexes assigned to the vibrational bond between the oxygen ion and the octahedral metal ion O–M_{octa} and the band ν_t around 600 cm^{-1} is attributed to the intrinsic vibrations of tetrahedral complexes between the oxygen ion and the tetrahedral metal ion O–M_{tetra} [18,19] .The band around 200 cm^{-1} is assigned to the divalent tetrahedral vibrations and the low-frequency band around 350 cm^{-1} is related to the divalent octahedral metal-oxygen ion complex [19–21]. In ferrites, metal cations are positioned according to the geometric configuration of the oxygen ion nearest neighbors in two different sub-lattices, tetrahedral and octahedral sites. The change in bond length of Fe^{3+}–O^{2-} at tetrahedral (0.189 nm) and octahedral (0.199 nm) sites cause a difference in band positions in different ratio. The strong frequency bands; ν_t = 609.07 cm^{-1} and ν_o 387.92 cm^{-1} in FTIR spectra of all samples are associated to the characteristics bands for the inverse-spinel structure [7]. The increase in substituents contents affect the grain size and density, which is attributed to the preparation conditions. Higher atomic mass of substituents contents show a shift towards lower frequency region in the characteristic of metal–oxygen stretching bands.

The cubic octahedral shape $Co_{1-x}Cu_xFe_{2-x}Al_xO_4$ ($0.0 \leq x \leq 0.8$) nanoparticles with diameter in range of 21 to 26.5 nm are observed in Transmission electron microscope (TEM) micrographs as presented in Fig. 5, which are in good agreement with the XRD analysis as listed in Table 2. The ferrite nanoparticles are uniform in both morphology and crystalline size but agglomerated to some extent which suggests the presence of high magnetic dipole interaction among the ferrite nanoparticles. It is expected that the average grain size decreases with increase in dopant Cu-Al substitution. When the Fe^{3+} ions in ferrite lattices are substituted by Al^{3+} ions, the lattice parameters are modified and variation of lattice parameter leads to lattice strains and cause internal stress [4,22]. The presence of α-Fe_2O_3 phase at the boundary of grain raises pressure on the grain and hinder the growth [4] .

Fig. 6 shows the hysteresis curves obtained at a field of 15 kOe of the synthesized nanoparticles for different Cu-Al substitution ratios at room temperature. The narrow loops indicate the soft nature of the ferrite nanomaterials.

With increase in Cu-Al contents, the value of M_s decreases from 80 to 25 emu/g and the coercive field increases from 148 to 608 Oe. The bulk value saturation magnetization for the single crystalline cobalt ferrite is 93.3 emu/g whereas the saturation magnetization 80 emu/g measured for synthesized cobalt ferrite nano-powder is much lower as compared to bulk value [4]. A comparison in variations of magnetic properties (M_s and H_c) of cobalt ferrite powders synthesized by different methods is summarized in Table 3, which depends on different factors [4,23].

With increase in Cu-Al concentration, a linear decrease in the saturation magnetization is observed as the tetrahedral and octa-

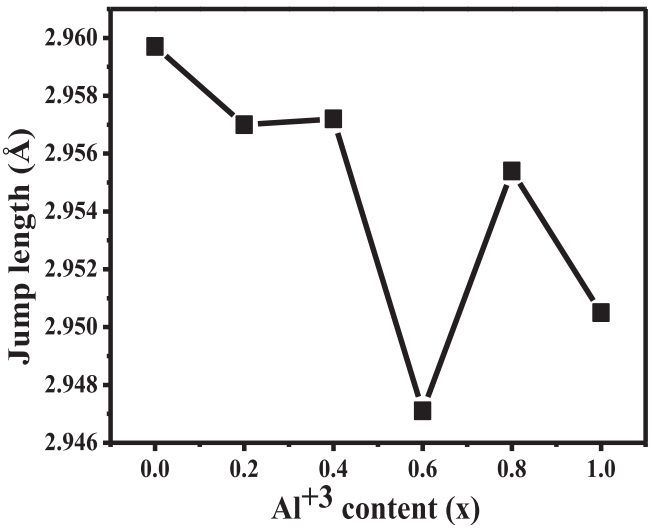

Fig. 3. Variation of jump length (L) with Cu^{2+}-Al^{3+} content x.

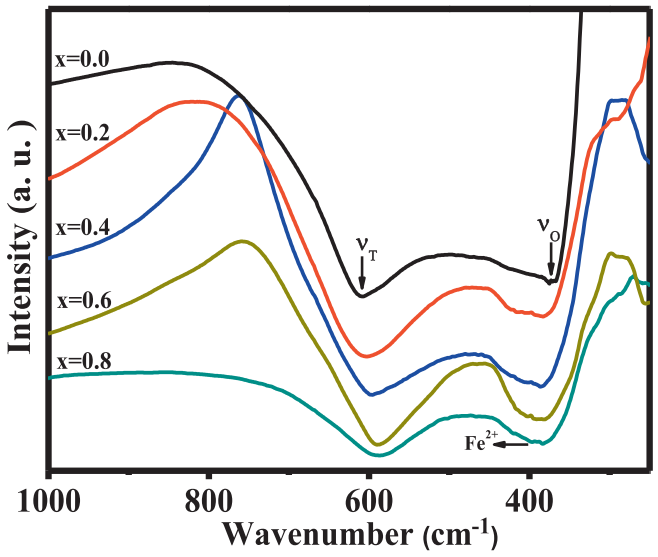

Fig. 4. Infrared spectra of $Co_{1-x}cu_xfe_{2-x}$ al_xo_4 nano-particles.

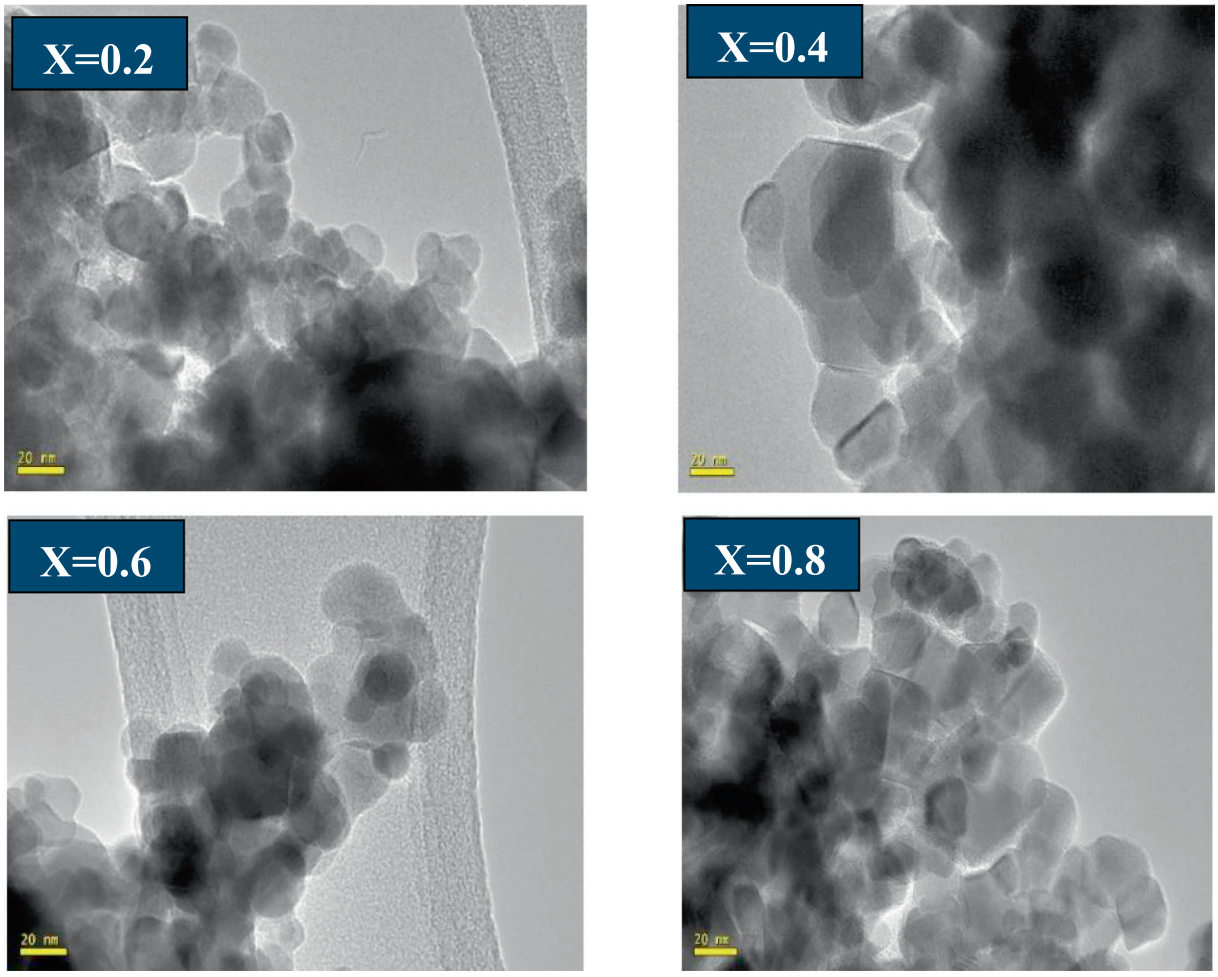

Fig. 5. Transmission electron microscope (TEM) images of $Co_{1-x}Cu_xFe_{2-x}$ Al_xO_4 nano-particles.

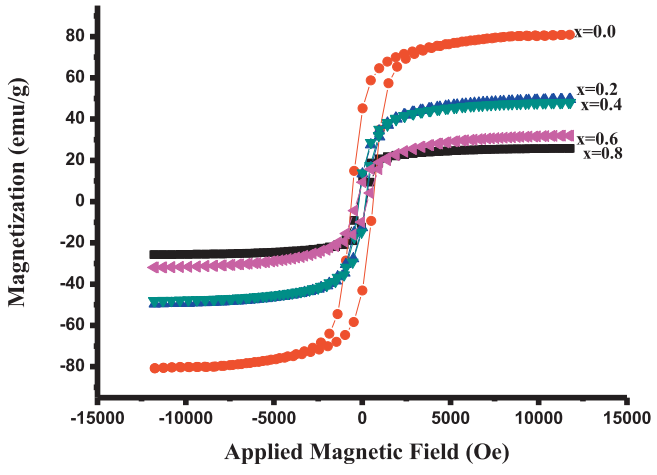

Fig. 6. Variation of magnetization (M_s) with applied field (H) of $Co_{1-x}Cu_xFe_{2-x}$ Al_xO_4 nano-particles.

hedral sites interaction is strongest and dominating over the octahedral-octahedral and tetrahedral-tetrahedral sites interactions. With increase in the Cu^{2+} and Al^{3+} contents, the crystallite size is decreased whereas, spin canting is increased due to increase in the substitution of of Fe^{3+} and Co^{2+} at tetrahedral and octahedral sites (redistribution of cations between 16 the tetrahedral and octahedral sites). As Cu^{2+}- Al^{3+} ions occupy both tetrahedral and octahedral sites, it expels Fe^{3+} from the octahedral sites, due to the charge compensation mechanism, thus leading to a slight overall decrease in M_s. In addition, the preferential occupancy of Cu^{2+} ions in the octahedral sites of the ferrite spinel, results a decrease in the concentration of Co^{2+} and Fe^{3+} ions at these sites. The measured magnetic moment of Co^{2+} and Fe^{3+} cations is 8 μ_b, which is greater than that of Cu^{2+} and Al^{3+} ions magnetic moment 1 μ_b [30]. The net result is a decrease in magnetic moment on both sub-lattices because of magnetic spin of neighboring tetrahedral and octahedral sites, which are anti-ferromagnetically coupled due to super exchange interaction in ferrite lattice. [18]. Thus, with increase in Cu-Al concentration, the net magnetic moment of the spinel ferrite decreases. The FTIR spectra of $Co_{1-x}Cu_xFe_{2-x}$ Al_xO_4 for x = 0.8 indicates the presence of Fe ions in its divalent state (Fe^{2+}) instead of the trivalent state (Fe^{3+}), therefore, a decrease in the value of the magnetization is due to existence of Fe^{2+} ions at octahedral sites [19].

In synthesized Cu-Al substituted cobalt ferrite nano-particles, the Co^{2+} ions migrates from octahedral to tetrahedral site. The magnetic moment (n_{bobs}) formula is calculated from Neel's two sublattice model using the relation in the Bohr magneton (μ_b) using molecular weight and saturation magnetization of each composition. The magnetic moment decreases with increase in Cu-Al ions ratio in each sub lattice and the calculated magnetic moment and observed values of the magneton number are in good agreement as illustrated in Fig. 7.

Table 3
Comparison of M_s and H_c of pure cobalt ferrite particles prepared by different synthesis methods and co-precipitation method.

M_s(emu/g)	H_c(Oe)	T °C	Synthesis Rout	Refs.
80	1374	850	Complex metric synthesis	[24]
79	1092	800	Mechanical milling	[25]
73	1005	800	Sol–gel auto-combustion	[26]
85	300	1000	Sol–gel	[27]
38	1597	80	Co-precipitation	[28]
52	1592	400	Auto combustion	[29]
80	608	900	Co-precipitation	Current work

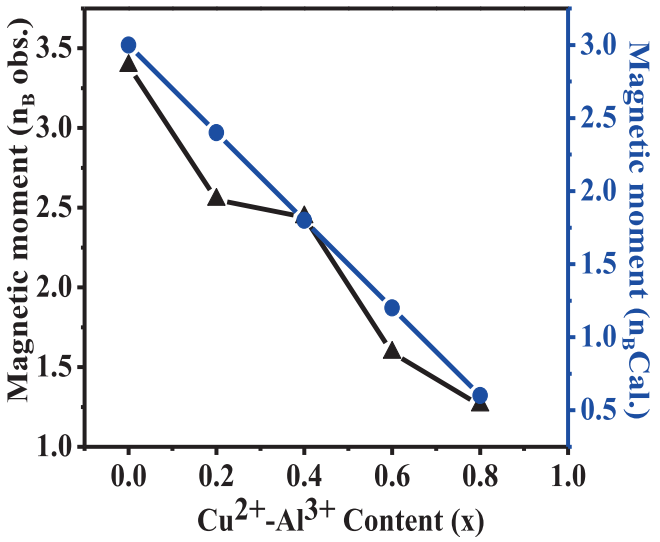

Fig. 7. Variation of observed (Obs.) And calculated (Cal.) Magneton number with Cu^{2+}-Al^{3+} content x.

All the prepared $Co_{1-x}Cu_xFe_{2-x}Al_xO_4$ $(0.0 \leq x \leq 0.8)$ nano-particles present soft magnetic characteristics with coercivity of a few hundred oersteds [31] due to substitution of Co and Fe by Cu-Al [19]. The decrease in coercive field leads to the reduction of the magnetocrystalline anisotropy of cobalt ferrite which is attributed to the decrease in the concentration of cobalt-iron contents and possesses highest magnetocrystalline anisotropy. The observed values of anisotropy-ranges from 1.96×10^5 J/m^3 for x = 0.0–0.29 $\times$ 10^5 J/m^3 for x = 0.8. The crystallite size decreases from 26 for x = 0.0 to 23 nm for x = 0.8 and coercivity decreases from 608 Oe for x = 0.0–244 Oe for x = 0.8. The coercive field has a large distribution due to its sensitivity to the particle agglomeration, whereas the squareness fluctuates in a narrower range depends on specific heat treatment temperature. As, the high-density data storage devices require saturation magnetization as high as possible and coercivity around 600 Oe, therefore, the small values of coercive field (H_c) of synthesized nano-ferrite makes these particles suitable for high density data storage devices.

Conclusion

Copper-Aluminum (Cu-Al) substituted Cobalt Ferrite nano-powders, $Co_{1-x}Cu_xFe_{2-x}Al_xO_4$ $(0.0 \leq x \leq 0.8)$, with optimized magnetic properties are synthesized using co-precipitation method. Cu-Al substitution has strong effect on the structural parameters of ferrite nano-particles. The lattice parameters such as lattice constant, cell volume and crystallite size are appreciably enhanced by increasing Cu-Al contents in cobalt ferrites. The saturation magnetization (Ms) and coercivity (H_c) of the $Co_{1-x}Cu_xFe_{2-x}Al_xO_4$ $(0.0 \leq x \leq 0.8)$ has been observed in the range of 25–80 emu/g and 184–608 Oe, respectively, associated with soft ferrite regime which are suitable for high density data storage application. The lattice constant is increased from 8.344 Å (x = 0.0) to 8.379 Å (x = 0.4) as the Cu-Al contents are increased. A decrease in magnetic moment on both sub-lattices (tetrahedral and octahedral) is due to magnetic spin of neighboring sites, which are anti-ferromagnetically coupled due to super exchange interaction in ferrite lattice.

Acknowledgments

We would like to thank Ibnu Sina Institute for Scientific and Industrial Research (ISI-SIR), Universiti Teknologi Malaysia (UTM) for providing research facilities. This research work has supported by PDRU (03E47, 03E22) and Tier 1 (12H82) Grants.

References

[1] Dippong T, Cadar O, Levei EA, Bibicu I, Diamandescu L, Leostean C, Lazar M, Borodi G, Tudoran LB. Structure and magnetic properties of $CoFe_2$ O_4/SiO_2 nanocomposites obtained by sol-gel and post annealing pathways. Ceram Int 2017;43:2113–22.
[2] Sajjia M, Oubaha M, Prescott T, Olabi A. Development of cobalt ferrite powder preparation employing the sol–gel technique and its structural characterization. J Alloy Compd 2010;506:400–6.
[3] Hashim M, Kumar S, Shirsath SE, Kotnala R, Shah J, Kumar R. Synthesis and characterizations of Ni_2^+ substituted cobalt ferrite nanoparticles. Mater Chem Phys 2013;139:364–74.
[4] Dabagh S, Ati AA, Rosnan R, Zare S, Othaman Z. Effect of Cu–Al substitution on the structural and magnetic properties of Co ferrites. Mater Sci Semicond Process 2015;33:1–8.
[5] Karimi Z, Mohammadifar Y, Shokrollahi H, Asl SK, Yousefi G, Karimi L. Magnetic and structural properties of nano sized Dy-doped cobalt ferrite synthesized by co-precipitation. J Magn Magn Mater 2014;361:150–6.
[6] Monaji VR, Das D. Influence of Zr doping on the structural, magnetic and magnetoelastic properties of cobalt-ferrites. J Alloy Compd 2015;634:99–103.
[7] Zare S, Ati AA, Dabagh S, Rosnan RM, Othaman Z. Synthesis, structural and magnetic behavior studies of Zn–Al substituted cobalt ferrite nanoparticles. J Mol Struct 2015;1089:25–31.
[8] Sontu UB, Yelasani V, Musugu VRR. Structural, electrical and magnetic characteristics of nickel substituted cobalt ferrite nano particles, synthesized by self combustion method. J Magn Magn Mater 2015;374:376–80.
[9] Ahmad I, Abbas T, Ziya AB, Abbas G, Maqsood A. Size dependent structural and magnetic properties of Al substituted Co–Mg ferrites synthesized by the sol–gel auto-combustion method. Mater Res Bull 2014;52:11–4.
[10] Raut AV, Barkule RS, Shengule DR, Jadhav KM. Synthesis, structural investigation and magnetic properties of Zn2+ substituted cobalt ferrite nanoparticles prepared by the sol–gel auto-combustion technique. J Magn Magn Mater 2014;358–359:87–92.
[11] Praveena K, Srinath S. Synthesis and characterization of $CoFe_2O_4$/Polyaniline nanocomposites for electromagnetic interference applications. J Nanosci Nanotechnol 2014;14:4371–6.
[12] Kannan YB, Saravanan R, Srinivasan N, Praveena K, Sadhana K. Structural, magnetic and optical characterization of $Ni0.8Zn0.2Fe_2O_4$ nano particles prepared by co-precipitation method. Physica B 2016;502:181–6.
[13] Kale A, Gubbala S, Misra R. Magnetic behavior of nanocrystalline nickel ferrite synthesized by the reverse micelle technique. J Magn Magn Mater 2004;277:350–8.
[14] Mustafa G, Islam MU, Zhang W, Anwar AW, Jamil Y, Murtaza G, Ali I, Hussain M, Ali A, Ahmad M. Influence of the divalent and trivalent ions substitution on the structural and magnetic properties of Mg0.5−xCdxCo0.5Cr0.04TbyFe1.96−yO4 ferrites prepared by sol–gel method. J Magn Magn Mater 2015;387:147–54.
[15] Panda RK, Muduli R, Kar SK, Behera D. Dielectric relaxation and conduction mechanism of cobalt ferrite nanoparticles. J Alloy Compd 2014;615:899–905.
[16] Tirupanyam B, Srinivas C, Meena S, Yusuf S, Kumar AS, Sastry D, Seshubai V. Investigation of structural and magnetic properties of co-precipitated Mn–Ni

ferrite nanoparticles in the presence of α-Fe_2 O_3 phase. J Magn Magn Mater 2015;392:101–6.
[17] Beji Z, Smiri L, Yaacoub N, Greneche J-M, Menguy N, Ammar S, Fievet F. Annealing effect on the magnetic properties of polyol-made Ni−Zn ferrite nanoparticles. Chem Mater 2010;22:1350–66.
[18] Hussein SI, Elkady AS, Rashad MM, Mostafa AG, Megahid RM. Structural and magnetic properties of magnesium ferrite nanoparticles prepared via EDTA-based sol–gel reaction. J Magn Magn Mater 2015;379:9–15.
[19] Rais A, Taibi K, Addou A, Zanoun A, Al-Douri Y. Copper substitution effect on the structural properties of nickel ferrites. Ceram Int 2014;40:14413–9.
[20] Balavijayalakshmi J, Suriyanarayanan N, Jayaprakash R. Role of copper on structural, magnetic and dielectric properties of nickel ferrite nano particles. J Magn Magn Mater 2015;385:302–7.
[21] Elkady AS, Hussein SI, Rashad MM. Structural and magnetic properties of Gd3+ ion substituted magnesium ferrite nanopowders. J Magn Magn Mater 2015;385:70–6.
[22] Praveena K, Sadhana K, Matteppanavar S, Liu H-L. Effect of sintering temperature on the structural, dielectric and magnetic properties of Ni0.4Zn0.2Mn0.4Fe_2O_4 potential for radar absorbing. J Magn Magn Mater 2017;423:343–52.
[23] Ati AA, Othaman Z, Samavati A, Doust FY. Structural and magnetic properties of Co–Al substituted Ni ferrites synthesized by co-precipitation method. J Mol Struct 2014;1058:136–41.
[24] Thang PD, Rijnders G, Blank DH. Spinel cobalt ferrite by complexometric synthesis. J Magn Magn Mater 2005;295:251–6.
[25] Rafferty A, Prescott T, Brabazon D. Sintering behaviour of cobalt ferrite ceramic. Ceram Int 2008;34:15–21.
[26] Coey JMD. Noncollinear spin arrangement in ultrafine ferrimagnetic crystallites. Phys Rev Lett 1971;27:1140.
[27] Singhal S, Namgyal T, Bansal S, Chandra K. Effect of Zn substitution on the magnetic properties of cobalt ferrite nano particles prepared via sol-gel route. J Electromagn Anal Appl 2010;2010.
[28] Cedeño-Mattei Y, Perales-Perez O, Tomar M, Roman F, Voyles P, Stratton W. Tuning of magnetic properties in cobalt ferrite nanocrystals. J Appl Phys 2008;103. 07E512-507E512-513.
[29] Yadav RS, Havlica J, Kuřitka I, Kozakova Z, Palou M, Bartoníčková E, Boháč M, Frajkorová F, Masilko J, Kalina L. Magnetic Properties of dysprosium-doped cobalt ferrite nanoparticles synthesized by starch-assisted Sol-Gel auto-combustion method. J Supercond Novel Magn 2015:1–11.
[30] Srinivas C, Tirupanyam B, Meena S, Yusuf S, Babu CS, Ramakrishna K, Potukuchi D, Sastry D. Structural and magnetic characterization of co-precipitated $Ni_xZn_{1-x}Fe_2O_4$ ferrite nanoparticles. J Magn Magn Mater 2016;407:135–41.
[31] Gul I, Pervaiz E. Comparative study of $NiFe_{2-x}$ Al_xO_4 ferrite nanoparticles synthesized by chemical co-precipitation and sol–gel combustion techniques. Mater Res Bull 2012;47:1353–61.